RESEARCH ARTICLE | MAY 24 2024

Synthesis and characterization Fe doped $BaBi_4Ti_4O_{15}$ prepared via molten salt method FREE

Dwi Nurcahyaningtyas; Anton Prasetyo

AIP Conf. Proc. 3106, 020005 (2024)
https://doi.org/10.1063/5.0214994

Synthesis and Characterization Fe Doped $BaBi_4Ti_4O_{15}$ Prepared via Molten Salt Method

Dwi Nurcahyaningtyas and Anton Prasetyo[a)]

Department of Chemistry, Faculty of Science and Technology, Universitas Islam Negeri Maulana Malik Ibrahim Malang, Jalan Gajayana 50 Malang, East Java, Indonesia 65144

[a)] *Corresponding author: anton@kim.uin-malang.ac.id*

Abstract. The four-layer Aurivillius compound $BaBi_4Ti_4O_{15}$ is reportedly applied as photocatalyst material with a band gap energy of 3.2 eV (387.5 nm). As a result, it works in the ultraviolet light range. The strategy to expand its work function is to decrease the band gap energy by doped with metal elements like Fe atoms. In this research, we synthesised Fe-doped $BaBi_4Ti_4O_{15}$ ($BaBi_4Ti_{3.95}Fe_{0.05}O_{15}$; $BaBi_4Ti_{3.90}Fe_{0.1}O_{15}$; $BaBi_4Ti_{3.85}Fe_{0.15}O_{15}$; and $BaBi_4Ti_{3.80}Fe_{0.2}O_{15}$) with the purposes to decreases its band gap energy. The diffractogram of samples showed the doped $BaBi_4Ti_4O_{15}$ compound was successfully formed and had no impurity phase with space group $A2_1am$. Micrograph scanning electron microscopy (SEM) showed plate-like morphology particles and still found agglomeration occurs. The result calculation of Kubelka-Munk showed that Fe doped can decrease the band gap energy of $BaBi_4Ti_4O_{15}$.

INTRODUCTION

Aurivillius compounds have a general formula $(Bi_2O_2)^{2+}$ $(A_{m-1}B_mO_{3m+1})^{2-}$ and consist of a bismuth layer $(Bi_2O_2)^{2+}$ and *pseudo-perovskite* layer $(A_{m-1}B_mO_{3m+1})^{2-}$, with m is the number of perovskite layers [1]. A is monovalent, divalent, and trivalent cations (K^+, Na^+, Ba^{2+}, Ca^{2+}, Sr^{2+}, Pb^{2+}, or Bi^{3+}), while B is tetravalent, pentavalent, hexavalent, or metals transision (Ti^{4+}, Nb^{5+}, Ta^{5+}, atau W^{6+}) [2]. Aurivillius compounds have some interesting properties, such as Ferroelectric [3], photocatalyst [4], piezoelectric [5], and photoluminescence [6]. Some Aurivillius compound opportunity as a photocatalyst material such as $BaBi_4Ti_4O_{15}$ [7], $Bi_5Ti_3CrO_{15}$ [8], $Bi_4V_2O_{11}$ [9], $Bi_{4.15}Nd_{0.85}Ti_3FeO_{15}$ [10], $Bi_2ASrTi_2TaO_{12}$ (A= Bi, La) [11], and Bi_3TiNbO_9 [12]. Four layers of Aurivillius compound $BaBi_4Ti_4O_{15}$ (BBT) are reported to be applied as photocatalyst material but have a high band gap energy of 3.2 eV (387.5 nm) [7]. Qi et al. (2019) reported the BBT compound was able to degrade 15% rhodamine B under ultraviolet-visible light for 3.5 h [7].

To expand the work function of BBT in the visible light range can be done by decreases its band gap energy. One technique to decrease band gap energy is doped with metal elements such as Ni [13], La [14], Co [15], Fe, Nb [16], Cr [17], W [18], and Mn [19]. The application of Fe metal as a dopant of material photocatalyst of Aurivillius compound has been studied by Liu et al. (2016) and resulted that Fe^{3+} doped $Bi_4Ti_3O_{12}$ have low band gap energy. As a result, it can work in the visible light region [20], and Yang et al. (2020) reported that Fe (III) dopant can decrease the band gap energy of Bi_2MoO_6 and show the wavelength shift in the visible light region [21].

The molten salt method (MSS) is one of the synthesis methods that produced a unique morphology of the Aurivillius compound. In addition, MSS has some advantages such as a) high homogeneity, b) high product purity, c) can control particle size [22], f) environmentally friendly, simple salt can be easily applied and removed [23], can be control morphology [24], using low temperature and short reaction duration [25]. Gu et al. (2011) successfully synthesised $BaBi_4Ti_4O_{15}$ via the molten salt method of K_2SO_4/Na_2SO_4 with plate-like morphology [26]. Materials with plate-like morphology have prospect as photocatalysts because they have a good active face and a great potential applied to photocatalyst activity of a semiconductor [27], and then the plate-like morphology shortens migration distance of e^-/h^+ pairs to reactive sites, and the result can increase photocatalyst activity in visible-light region [28]. They also reported that obtaining a unique morphology is expected to increase the photocatalyst activity of $BaBi_4Ti_4O_{15}$. Based on the description in this research, synthesised Fe-doped $BaBi_4Ti_4O_{15}$ compound ($BaBi_4Ti_{3.95}Fe_{0.05}O_{15}$; $BaBi_4Ti_{3.90}Fe_{0.1}O_{15}$; $BaBi_4Ti_{3.85}Fe_{.15}O_{15}$; $BaBi_4Ti_{3.80}Fe_{0.2}O_{15}$).

The 6th International Conference on Mathematics and Science Education (ICoMSE) 2022
AIP Conf. Proc. 3106, 020005-1–020005-8; https://doi.org/10.1063/5.0214994
Published under an exclusive license by AIP Publishing. 978-0-7354-4958-9/$30.00

EXPERIMENTAL SECTION

Precursors and Tools

The chemicals used in this research are $BaCO_3$ (Merck, 99.9%), Bi_2O_3 (Sigma Aldrich, 99.9%), TiO_2 (Sigma Aldrich, 99.9%), Fe_2O_3 (Sigma Aldrich, 99.9%), and Na_2SO_4/K_2SO_4 salt (Merck 99.9%). The samples of the product were characterised by *X-ray* diffraction (Rigaku Miniflex Diffractometer) on 2θ (°)= 3-90, scanning electron microscopy-energy dispersive spectroscopy (Hitachi Flexsem 100) with magnification 5 μm, and ultraviolet-visible diffuse reflectance spectroscopy (Thermo Evolution 220) with wavelength 200-800 nm.

Synthesis of $BaBi_4Ti_4O_{15}$

The synthesis compound target is 3 grams, and the requirement of precursors was calculated based on stoichiometry calculation tabulated in TABLE 1. All precursors were mixed and ground mixed ground-grinded for 1 h and add acetone to maximise homogeneity, and then calcined at 850 and 870°C, respectively, for 6 h. After that, the products were washed by hot water to remove the salt, and dry it using the oven.

TABLE 1. Mass of all precursor synthesis of Fe-doped $BaBi_4Ti_4O_{15}$.

Compound target	Mass target (gram)	Precursor mass (gram)					
		$BaCO_3$ (gram)	Bi_2O_3 (gram)	TiO_2 (gram)	Fe_2O_3 (gram)	Na_2SO_4 (gram)	K_2SO_4 (gram)
$BaBi_4Ti_{3,95}Fe_{0,05}O_{15}$	3	0.4213	1.9888	0.6737	0.0085	2.1226	2.6042
$BaBi_4Ti_{3,90}Fe_{0,1}O_{15}$	3	0.4211	1.9883	0.6650	0.0170	2.1220	2.6034
$BaBi_4Ti_{3,85}Fe_{0,15}O_{15}$	3	0.4210	1.9877	0.6563	0.0255	2.1214	2.6027
$BaBi_4Ti_{3,80}Fe_{0,2}O_{15}$	3	0.4209	1.9872	0.6476	0.0340	2.1208	2.6020

Characterization

The sample product was characterized using (a). *X-ray* diffraction (XRD) technique to identify phase formed on 2θ (°)= 3-90. The diffractogram was compared using standard data $BaBi_4Ti_4O_{15}$ in the ICSD database. Then, the diffractogram was refined using Rietica software with the Le-Bail method. (b). scanning electron microscopy-energy dispersive spectroscopy (SEM-EDS) to know the morphology and constituent elements of the compound. (c). ultraviolet-visible diffuse reflectance spectroscopy (UV-Vis DRS) to understand absorbance and reflectance with wavelength 200-800 nm to get absorbance spectra and calculated using Kubelka-Munk equation to get bandgap energy. The Kubelka-Munk equation is $(R)= (\frac{(1-R)^2}{2R} = \frac{K}{S})$. $F(R)$ is the Kubelka-Munk factor, K is the molar absorption coefficient, S is the scattering coefficient, and R is the absolute reflectance [29].

RESULT AND DISCUSSION

The Diffractogram of Fe-doped $BaBi_4Ti_4O_{15}$ is shown in Figure 1 (a) and matched with the $BaBi_4Ti_4O_{15}$ standard on International Crystallography Standard Data (ICSD) Number. 150928 with space group $A2_1am$ (orthorhombic class). The typical peaks $BaBi_4Ti_4O_{15}$ compound found on 2θ= 16.9; 21.2; 23.1; 30; 32.7; 39.3; 47; 51.5; and 56.8° showed the targed compound have been formed. The diffractogram showed the absence of additional peaks, indicating there are no impurities. The addition of Fe dopant in $BaBi_4Ti_4O_{15}$ caused a diffraction shift peak at 2θ= 30° (Figure 1 (b)) and showed the changes of lattice parameters and cell volume due to the change ionic radii of dopant as a result of the doped mechanism (the ionic radii of Fe^{3+} are 0.064 nm and Ti^{4+} is 0.068 nm) [30, 31].

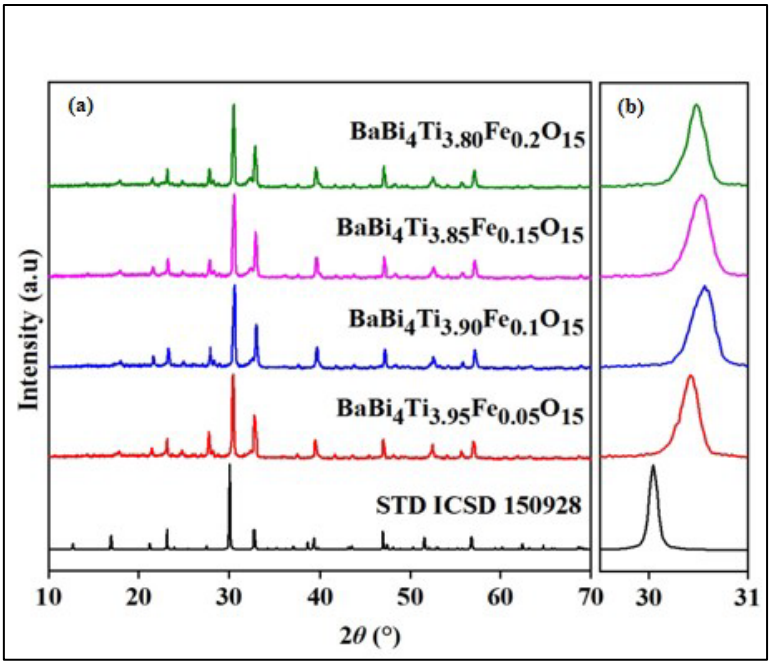

FIGURE 1. (a) The diffractogram of Fe doped $BaBi_4Ti_4O_{15}$ and (b) Diffraction peak shift of 2θ= 30°. (The figure is result of independent characterization in Greenlabs Indonesia Utama, Bandung).

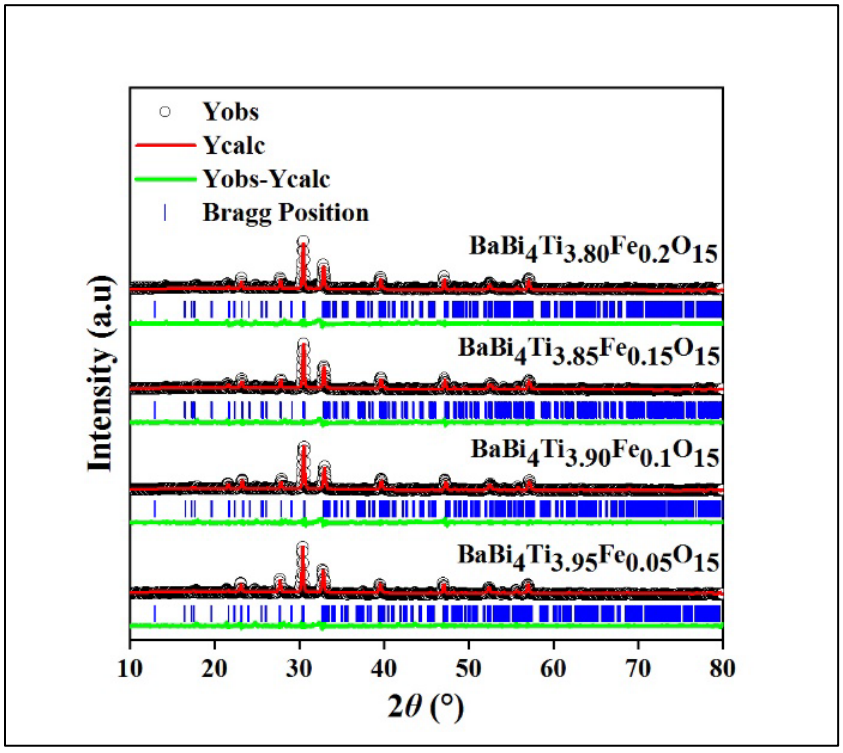

FIGURE 2. The refinement plot of Fe-doped $BaBi_4Ti_4O_{15}$.

Figure 2 shows the refinement plot, and its result is summarized in TABLE 2. The refinement process used the standard data $BaBi_4Ti_4O_{15}$ ICSD Number. 150928 which has an orthorombic crystal system with space group $A2_1am$, azimetric unit (Z)= 4, lattice parameter a= 5.4707, b= 5.4565, c= 41.865 and α=β=γ=90°. Lattice parameters *a, b, c* and cell volume changed after the addition of Fe dopant as a result of changes in ionic radii. *Rp* and *Rwp* values shown

in the range 13-15 indicate that the diffractogram of the sample is a high match with the standard [32]. The addition of Fe dopant did not change the crystal system and space group of the sample [33]. However, the change of crystal lattice $a=b=c$ and crystal volume did not linear as a function of Fe doped concentration. It may be that high-temperature synthesis caused the valency number of Fe change.

TABLE 2. The result of refinement diffractogram of Fe doped $BaBi_4Ti_4O_{15}$.

Parameter	$BaBi_4Ti_4O_{15}$ STD. ICSD No. 150928	Fe Doped $BaBi_4Ti_4O_{15}$			
		$BaBi_4Ti_{3.95}Fe_{0.05}O_{15}$	$BaBi_4Ti_{3.90}Fe_{0.1}O_{15}$	$BaBi_4Ti_{3.85}Fe_{0.15}O_{15}$	$BaBi_4Ti_{3.80}Fe_{0.2}O_{15}$
Crystal system	Orthorhombic	Orthorhombic	Orthorhombic	Orthorhombic	Orthorhombic
Space group	$A2_1am$	$A2_1am$	$A2_1am$	$A2_1am$	$A2_1am$
Azimetric unit (Z)	4	4	4	4	4
a (Å)	5.4707 (2)	5.4668 (6)	5.4182 (5)	5.4407 (5)	5.4541 (6)
b (Å)	5.4565 (2)	5.4191 (9)	5.396 (1)	5.400 (1)	5.410 (1)
c (Å)	41.865 (11)	40.983 (5)	40.929 (4)	40.879 (4)	40.908 (5)
Cell volume (V)	1249.71	1214.1 (3)	1196.7 (3)	1200.9 (3)	1207.1 (3)
R_p (%)	-	14.28	13.82	13.58	14.02
R_{wp} (%)	-	14.38	13.86	13.91	15.44
GoF (X^2)	-	22.73	21.97	23.43	28.70

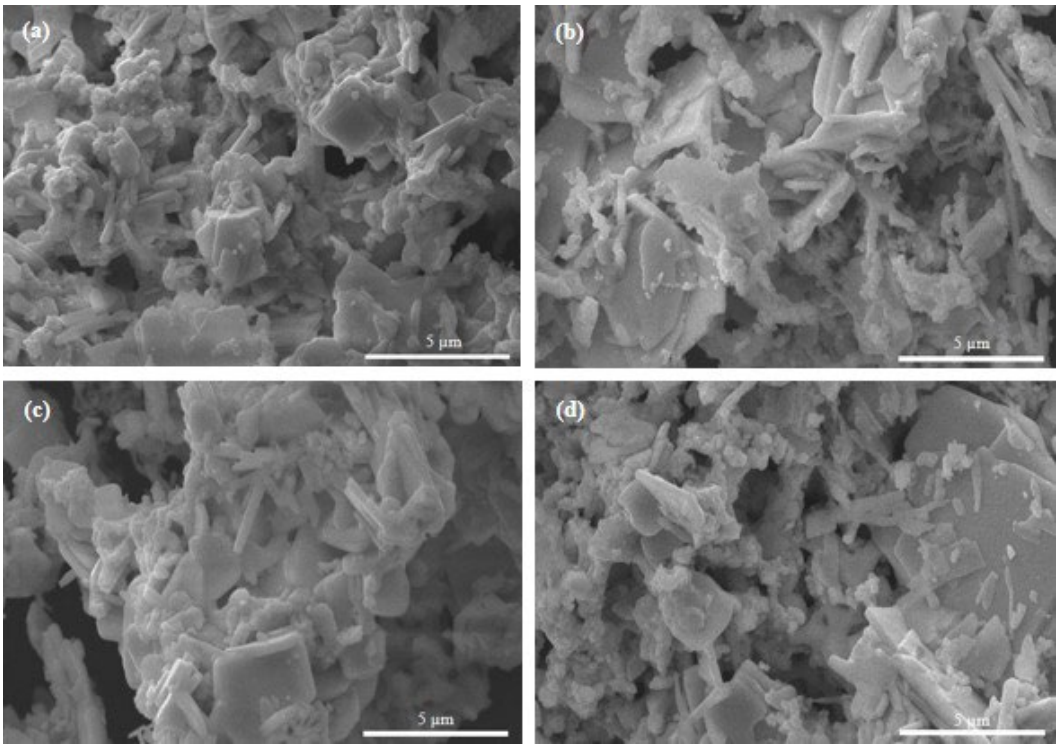

FIGURE 3. The sample micrograph of (a) $BaBi_4Ti_{3.95}Fe_{0.05}O_{15}$, (b) $BaBi_4Ti_{3.90}Fe_{0.1}O_{15}$, (c) $BaBi_4Ti_{3.85}Fe_{0.15}O_{15}$, (d) $BaBi_4Ti_{3.80}Fe_{0.2}O_{15}$. (The figure is result of independent characterization in mechanical engineering laboratory, Institut Teknologi Sepuluh Nopember, Surabaya).

Micrograph Fe doped $BaBi_4Ti_4O_{15}$ shown in Figure 3 with plate-like morphology similar to previous research [34]. The molten salt method is one of the effective methods for producing plate-like morphology in Aurivillius compounds. Gu et al. (2011) synthesised $BaBi_4Ti_4O_{15}$ using the molten salt method with mixed salt of Na_2SO_4/K_2SO_4 to produce a plate-like morphology [26]. The addition of Fe dopant in the $BaBi_4Ti_4O_{15}$ with variation 0.05, 0.1, 0.15, and 0.2 affect the morphology of the sample. The micrograph shows that agglomeration increases as the concentration of Fe dopant increases. The plate-like morphology is not uniform, and agglomeration occurs because gradual lattice distortion induced by Fe dopant causes the scattering of denser crystal grains [32]. In addition, the distortion occurs because the addition of dopant causes low sample crystallinity [33]. The EDS spectra are shown in Figure 4 and summarized in TABLE 3, which indicates the product synthesis contains constituent elements of the compound: Ba, Bi, Ti, Fe, and O. EDS spectra show Fe dopant increase, indicating dopant substituted in the sample.

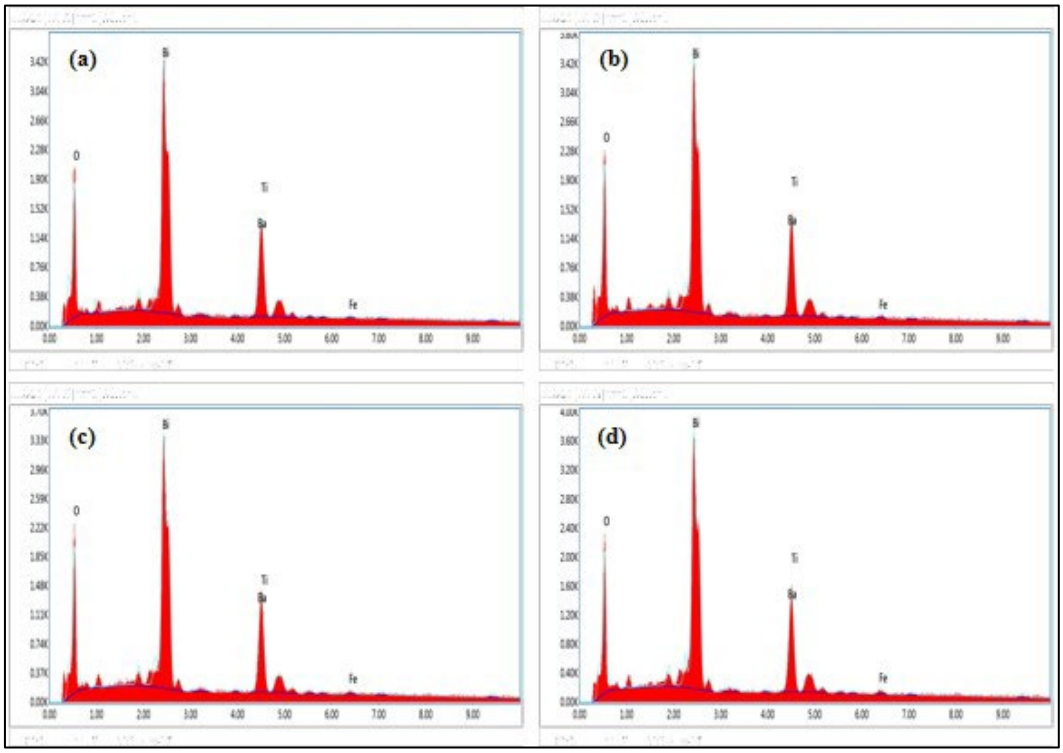

FIGURE 4. The EDS spectra of (a) $BaBi_4Ti_{3.95}Fe_{0.05}O_{15}$, (b) $BaBi_4Ti_{3.90}Fe_{0.1}O_{15}$, (c) $BaBi_4Ti_{3.85}Fe_{0.15}O_{15}$, (d) $BaBi_4Ti_{3.80}Fe_{0.2}O_{15}$. (The figure is result of independent characterization in mechanical engineering laboratory, Institut Teknologi Sepuluh Nopember, Surabaya).

TABLE 3. The EDS results.

Sample	Ba (% Weight)	Bi (% Weight)	Ti (% Weight)	Fe (% Weight)	O (% Weight)
$BaBi_4Ti_{3.95}Fe_{0.05}O_{15}$	17.30	47.94	15.20	1.35	18.21
$BaBi_4Ti_{3.90}Fe_{0.1}O_{15}$	15.81	46.85	15.87	1.94	19.53
$BaBi_4Ti_{3.85}Fe_{0.15}O_{15}$	17.47	47.12	14.77	2.02	18.62
$BaBi_4Ti_{3.80}Fe_{0.2}O_{15}$	17.56	47.44	14.78	2.20	18.02

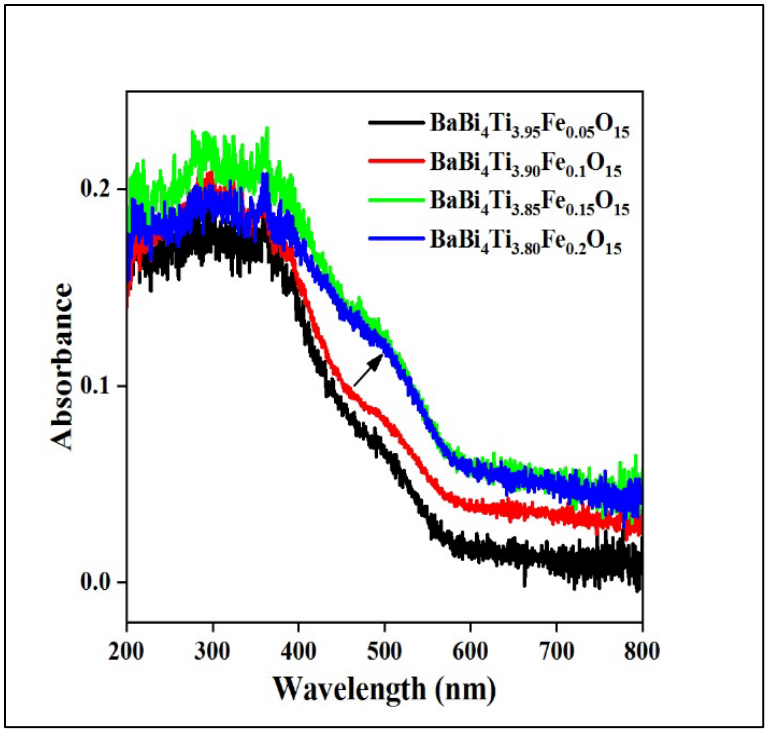

FIGURE 5. The UV-Vis DRS absorption spectra of Fe-doped $BaBi_4Ti_4O_{15}$. (The figure is result of independent characterization in chemistry laboratory of UIN Maulana Malik Ibrahim, Malang).

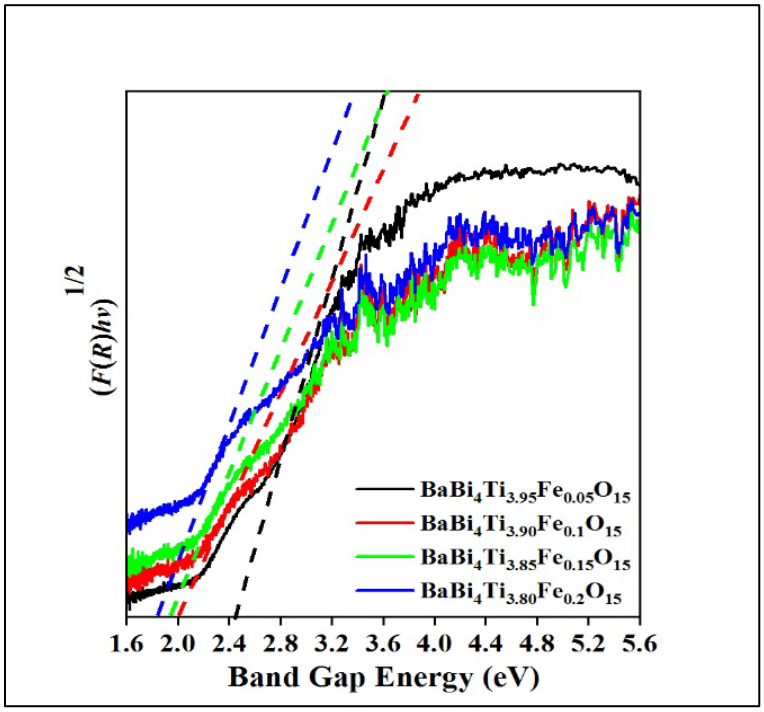

FIGURE 6. The Tauc-plot of Fe-doped $BaBi_4Ti_4O_{15}$. (The figure is result of independent characterization in chemistry laboratory of UIN Maulana Malik Ibrahim, Malang).

TABLE 4. The band gap energy of Fe-doped $BaBi_4Ti_4O_{15}$.

Sample	Band gap energy (eV)
$BaBi_4Ti_4O_{15}$ [7]	3.20
$BaBi_4Ti_{3.95}Fe_{0.05}O_{15}$	2.5821
$BaBi_4Ti_{3.90}Fe_{0.1}O_{15}$	1.9995
$BaBi_4Ti_{3.85}Fe_{0.15}O_{15}$	1.9295
$BaBi_4Ti_{3.80}Fe_{0.2}O_{15}$	1.8812

Absorbance spectra in the Fe-doped $BaBi_4Ti_4O_{15}$ shown in Figure 5 can be seen when adding a Fe dopant, which can increase the absorbance and shift to the visible light region. The Tauc plot of the doped $BaBi_4Ti_4O_{15}$ compound is shown in Figure 6, and the result of the band gap energy calculation is summarized in TABLE 4. Table 4 shows the addition of Fe dopant can affect the value of band gap energy as a result of new electronic transitions. The effect of Fe dopant concentration is inversely proportional to the band gap energy value; the higher the Fe dopant concentration, the smaller the band gap energy. It's due to the Fe dopant causing the formation of a new state in the electronic transition from the valance band (VB) to the conduction band (CB). In $BaBi_4Ti_4O_{15}$, the electronic transition occurs from O2p + Bi6s + Fe-t_{2g} (VB) to Ti-3d (CB) orbital, and the addition of Fe dopant resulted in a new electronic transition from O2p + Bi6s + Fe-t_{2g} (VB) to Fe-e_g (CB) orbitals [35].

CONCLUSION

The Fe-doped $BaBi_4Ti_4O_{15}$ compound was successfully synthesised with space group $A2_1am$, and there is no impurity. The micrograph shows the sample has a plate-like morphology that is not uniform, and agglomeration occurs. The UV-Vis DRS spectra indicated that the doped $BaBi_4Ti_4O_{15}$ compound showed decreased band gap energy as well as caused an absorbance shift to the visible light region.

ACKNOWLEDGEMENTS

Thank you to Department of Chemistry, Faculty Science and Technology, UIN Maulana Malik Ibrahim Malang for facilitating this research.

REFERENCES

1. P. Fang, P. Liu, and Z. Xi, Phys. B: Condens. Matter **33**, 1-20 (2015).
2. A. Bencan, P. Boullay, and J. P. Mercurio, Solid State Sci. **6**, 547-551 (2004).
3. Y. Ahn and J. Y. Son, MSEB. **266**, 1-5 (2021).
4. Y. Jiang, Y. Mi, C. Li, W. Fang, X. Li, X. Zeng, Y. Liu, and W. Shangguan, J. Alloys Compd. **884**, 1-6 (2021).
5. C. L. Diao, J. B. Xu, H. W. Zheng, L. Fang, Y. Z. Gu, and W. F. Zhang, Ceram. Int. **39**, 6991-6995 (2013).
6. D. Peng, H. Zou, C. Xu, X. Wang, and X. Yao, J. Alloys Compd. **552**, 463-468 (2013).
7. W. Qi, Y. Wang, J. Wu, Z. Hu, C. Jia, and H. Zhang, Adv. Appl. Ceram. **118**, 418-424 (2019).
8. Z. Gu, J. Qian, R. Wang, M. Lv, X. Xu, and C. Luo, J. Energy Chem. **62**, 572-580 (2021).
9. Y. Lu, Y. Pu, J. Wang, C. Qin, C. Chen, and H.I. Seo, Appl. Surf. Sci. **347**, 719-726 (2015).
10. T. Xiao, C. Guo, H. Wang, R. Zhang, Y. Li, W. Shao, Y. Zhang, X. Wu, J. Tan, and W. Ye, Mater. Lett. **127679**, 1-12 (2020).
11. D. Wang, K. Tang, Z. Liang, and H. Zheng, J. Solid State Chem. **183**, 361-366 (2010).
12. L. Jiang, S. Ni, G. Liu, and X. Xou, Appl. Catal. **12**, 1-32 (2017).
13. T. Wang, H. Deng, W. Zhou, S. Si, B. Guo, X. Zheng, P. Yang, and J. Chu, Mater. Lett. **47**, 1-9 (2018).
14. Z. Peng, X. Zeng, F. Cao, and X. Yang, J. Alloys Compd. **695**, 626-631 (2017).
15. Z. Yu, B. Yu, Y. Liu, P. Zhou, J. Jiang, K. Liang, Y. Lu, H. Sun, X. B. Chen, Z. Ma, T. Zhang, C. Huang, and Y. Qi, Ceram. Int. **22**, 1-20 (2017).
16. C. Lavado and M.G. Stachiotti, J. Alloys Compd. **731**, 914-919 (2018).
17. W. Yin, C. Chen, W. Bai, J. Yang, Y. Zhang, X. Tang, C. G. Duan, and J. Chu, Ceram. Int. Shanghai **42**, 4298-4305 (2016).
18. X. Zuo, M. Zhang, E. He, B. Guan, Y. Qin, J. Yang, X. Zhu, and J. Dai, J. Alloys Compd. **77**, 1-21 (2017).

19. Y. Tang, Z. Y. Shen, Q. Du, X. Zhao, F. Wang, X. Qin, T. Wang, W. Shi, D. Sun, Z. Zhou, and S. Zhang, J. Eur. Ceram. Soc. **25**, 1-23 (2018).
20. Y. Liu, G. Zhu, J. Ghao, M. Hojamberdiev, R. Zhu, X Wei, Q. Guo, and P. Liu, Appl. Catal. **69**, 1-34 (2016).
21. G. Yang, Y. Liang, K. Li, J. Yang, K. Wang, R. Xu, and X. Xie, J. Alloys Compd. **156231**, 1-44 (2020).
22. D. G. Porob and P. A. Maggard, Mater. Res. Bull. **41**, 1513-1519 (2006).
23. X. Ke, J. Cao, M. Zheng, Y. Chen, J. Liu, and G. Ji, Mater. Lett. **61**, 3901-3903 (2007).
24. Y. Huang, X. Liu, Y. Jiang, and X. Zhu, Ceram. Int. **47**, 11654-11661 (2021).
25. R. J. Liu, L. X. Yang, Y. Wang, H. J. Liu, S. L. Zhu, and C. L. Zheng, Ceram. Int. **47**, 16086-16093 (2021).
26. Y. J. Gu, J. L. Huang, L. H. Li, K. Zhang, X. Wang, Q. Li, X. H. Tan, and H. Xu, Mater. Sci. Forum. **687**, 333-338 (2011).
27. X. Zhao, H. Yang, S. Li, Z. Cui, and C. Zhang, MRB **18**, 1-31 (2018).
28. Y. Zhang, J. Gao, Z. Chen, and Z. Lu, Ceram. Int. **103**, 1-10 (2018).
29. J. Shen, Y. Li, and J. H. Le, Dyes Pigm. **127**, 187-188 (2016).
30. D. P. Song, J. Yang, Y. X. Wang, J. Yang, and X. B. Zhu, Ceram. Int. **136**, 1-5 (2017).
31. Q. Guo, Q. Wang, G. Chen, M. Shen, and B. Li, Mater **58**, 383-389 (2017).
32. B. M. Haque, D. B. Chandra, P. Jiban, I. Nurul, and Z. Abdullah, Mater. Sci. Semicond. **89**, 223-233 (2019).
33. W. T. Li, W. Z. Huang, H. Zhuo, H. Y. Yin, and Y. F. Zheng, Mater. Res. Bull. **64**, 432-437 (2015).
34. A. Chakrabarti, J. Bera, and T. P. Sinha, Phys. B: Condens. Matter **404**, 1498-1502 (2009).
35. X. Liu, L. Xu, Y. Huang, C. Qin, L. Qin, and H. J. Seo, Ceram. Int. **103**, 1-30 (2017).